Organic Electronics 51 (2017) 471–476

Contents lists available at ScienceDirect

Organic Electronics

journal homepage: www.elsevier.com/locate/orgel

Enhanced outcoupling in flexible organic light-emitting diodes on scattering polyimide substrates

Kyung Min Lee[a], Romain Fardel[b,c], Lianfeng Zhao[a], Craig B. Arnold[a,b,c], Barry P. Rand[a,d,*]

[a] Department of Electrical Engineering, Princeton University, Princeton, NJ 08544, United States
[b] Department of Mechanical and Aerospace Engineering, Princeton University, Princeton, NJ 08544, United States
[c] Princeton Institute for the Science and Technology of Materials (PRISM), Princeton University, Princeton, NJ 08544, United States
[d] Andlinger Center for Energy and the Environment, Princeton University, Princeton, NJ 08544, United States

ARTICLE INFO

Keywords:
Flexible organic light-emitting diodes
White organic light emitting devices
Outcoupling
Silver nanowires
Colorless polyimide
Scattering substrate

ABSTRACT

We demonstrate an upscalable approach to increase outcoupling in organic light-emitting diodes (OLEDs) fabricated on flexible substrates. The outcoupling enhancement is enabled by introducing a thin film of microporous polyimide on the backside of silver nanowire (AgNW) electrodes embedded in neat colorless polyimide. This porous polyimide film, prepared by immersion precipitation, utilizes a large index contrast between the polyimide host and randomly distributed air voids, resulting in broadband haze (> 75%). In addition, the composite polyimide/AgNW scattering substrate inherits the high thermal (> 360 °C), chemical, and mechanical stability of polyimides. The outcoupling efficiency of the composite scattering substrate is studied via optical characterization of the composite substrate and electron microscopy of the scattering film. The flexible scattering substrates compared to glass/indium tin oxide (ITO) allows for a 74% enhancement in external quantum efficiency (EQE) for a phosphorescent green OLED, and 68% EQE enhancement for a phosphorescent white OLED. The outcoupling enhancement remains unharmed after 5000 bending cycles at a 2 mm bending radius. Moreover, the color uniformity over viewing angles is improved, an important feature for lighting applications.

1. Introduction

White organic light-emitting diodes (OLEDs) are emerging solid-state lighting elements, offering unique advantages of high internal quantum efficiency [1–4] and facile large-area production on flexible substrates [5]. The challenges in producing practical flexible white OLEDs are twofold. First, transparent conducting electrodes (TCEs) must be realized on plastic substrates while simultaneously optimizing their optical, electrical, chemical, and mechanical properties. New classes of TCEs such as metallic nanowires [6–9], graphene [10,11], and carbon nanotubes [12,13] have been incorporated into flexible plastics to replace ITO, whose brittleness and high-temperature processing are generally incompatible with plastics. Second, effective light outcoupling structures should be introduced to these flexible OLEDs since only 20–30% of generated photons can escape an unmodified planar device, owing to surface plasmon polaritons at the metal-organic interface, waveguiding in the high-index organic stack, and internally reflected light at the substrate-air interface [14–16]. These challenges are exacerbated for white OLEDs as they also need to be addressed over the full visible spectrum. In addition, white OLEDs for general lighting are expected to meet an additional set of performance metrics such as a high color rendering index (CRI) and color uniformity across a large-area panel and between panels, as well as color uniformity over large viewing angles [17,18].

Various strategies have tackled these challenges and reported flexible monochromatic and/or white OLEDs with improved performance through the use of nanostructured metal grid-electrodes [19,20], nanotextured plastic substrates [21], microlens arrays combined with scattering nanoparticles [22], and planar substrates embedded with high-index scattering particles [23]. However, many of these outcoupling structures are realized by lithography and are difficult or too costly to upscale. A more scalable approach to extract both waveguiding and substrate losses was introduced in which simple oxygen plasma treatment was used to obtain micropatterned plastic substrates [24]. However, the application was limited to monochromatic OLEDs. We recently introduced a scalable and broadband alternative whereby porous polymer films are used on the substrate backside to outcouple substrate loss in both monochromatic and white OLEDs without costly lithography. The porous polymer film takes advantage of a large index contrast between itself (in that case, Kapton with $n > 1.7$) and non-absorbing air pockets, showing the ability to outcouple as much as 44% of substrate-trapped photons in a rigid glass/ITO structure [25]. The

* Corresponding author. Department of Electrical Engineering and Andlinger Center for Energy and the Environment, Princeton University, Princeton, NJ 08544, United States.
E-mail address: brand@princeton.edu (B.P. Rand).

http://dx.doi.org/10.1016/j.orgel.2017.09.042
Received 30 July 2017; Received in revised form 22 August 2017; Accepted 23 September 2017
Available online 25 September 2017
1566-1199/ © 2017 Elsevier B.V. All rights reserved.

porous polyimide films are produced via immersion precipitation in which a film cast from the polyimide precursor (polymer and solvent) is introduced to a coagulation bath containing a nonsolvent. Nonsolvent-induced phase inversion and solvent-nonsolvent exchange take place, and the polymer solidifies to a porous film [26]. The air voids formed spontaneously in this way are randomly distributed within the polyimide host, giving rise to broadband haze. In addition, Go et al. has shown that the choice of nonsolvent has a significant impact on the morphology and thickness of the resulting porous polymer film, and hence its outcoupling efficiency [27]. In this work, we use deionized water as our nonsolvent which is both scalable and highly miscible with our choice of solvent (N-methyl-2-pyrrolidone, NMP), thus accelerating the immersion precipitation process.

Here, we adopt the precipitation immersion principle to obtain microporous polyimide scattering films from colorless polyimide (CPI). Colorless polyimide is an optically transparent material that inherits the excellent thermal, mechanical, and chemical stability of aromatic polyimides. Unlike conventional polyimides such as Kapton that absorb strongly in the short visible wavelengths, CPIs have improved visible transmission by introducing alicyclic [28] or semialicyclic [29] substituents or highly electronegative substituents [30] in the synthesis. These substituents shift the absorption band edge of polyimides by inhibiting the formation of charge transfer complexes between the diamine (donor) and the dianhydride (acceptor) moieties [31]. In particular, CPI has proven to be an excellent host material for AgNWs, and composite CPI/AgNW substrates have a high electrical to optical conductivity ratio comparable to that of glass/ITO [7,32]. Moreover, thermal imidization of CPI with embedded AgNWs resulted in an exceptionally robust TCE resistant to scratching and tensile stress, as well as an ultra-smooth (< 1 nm root mean square roughness) active area, which is critical for preventing a common electrical failure mode (shorting) in large area thin-film devices [33]. As such, we use CPI/AgNW substrates as a platform to integrate the porous polyimide scattering film (pCPI) for outcoupling. By using CPI as both the substrate and the scattering film, we minimize reflection loss from any inherent index contrast as well as parasitic absorption loss in the short wavelengths, an aspect that is particularly important for white OLEDs.

2. Experimental

The preparation of the conductive and scattering flexible substrates is schematically illustrated in Fig. 1. As a first step, a random network of AgNWs (ACS Material) is deposited on a carrier substrate (Fig. 1a) via spin coating. The AgNWs are then patterned via pulsed UV laser ablation (Fig. S1) to define an active OLED area of 2 × 5 mm^2, and 30 μJ of 22 ns-pulse energy is sufficient to completely eject the AgNWs from the glass substrate. To protect the remaining AgNWs during thermal imidization [34], a titania (TiO_2) sol-gel is synthesized as in Ref. [7] and deposited via spin coating (Fig. 1c). A thin (~2 nm) layer of TiO_2 is sufficient to prevent AgNWs from breaking up into droplets, a process that occurs in nanowires at temperatures much below the melting point of bulk silver due to the Rayleigh-Plateau instability [35,36]. Then, colorless polyimide precursor solution (10 wt%) is blade coated and dried under vacuum for 40 min at 80 °C to remove most of the solvent (Fig. 1d). This CPI precursor is synthesized by polymerization of two equimolar moieties in NMP: 4,4′-oxydiphthalic anhydride (TCI America) and 2,2-bis[4-(4-aminophenoxy)pheny] hexafluoropropane (TCI America). The solution was stirred in a nitrogen-filled chamber for at least 24 h before use. For the outcoupling-enhanced scattering substrate, a freestanding pCPI film is obtained by spin coating the same CPI precursor solution (2 krpm for 90 s) on a glass substrate and immediately submerging the film for 20 min in a deionized water bath for immersion precipitation. The resulting pCPI film is then laminated to the backside of the dried CPI/TiO_2/AgNW (referred to as CPI/AgNW hereafter) stack prior to imidization to promote cross-linking of the CPI and pCPI end units and create a smooth, homogeneous interface (Fig. 1e). The full stack is then imidized (Fig. 1f) in a furnace (20 min at 160 °C followed by 20 min at 360 °C). At this stage, a freestanding pCPI/CPI/AgNW substrate is obtained by delaminating it from the carrier glass substrate (Fig. 1g). The scattering substrate prepared in this way consists of AgNWs embedded in a 50 μm-thick neat CPI film with a 6.3 μm-thick pCPI on the substrate backside, and the control substrate (CPI/AgNW) consists of AgNWs in a 50 μm thick neat CPI film. The optical characterization of the flexible substrates is conducted using an integrating sphere with a 350 W xenon lamp and a monochromator, in accordance with ASTM D1003-13. The sheet resistance of the substrates is measured with a custom four-point probe, and the morphology of the pCPI scattering layer is studied with FEI Helios NanoLab DualBeam (FIB/SEM) after coating the sample with 100 nm aluminum.

The CPI/AgNW substrates with and without the pCPI scattering layer were used to fabricate green and white phosphorescent OLEDs (PHOLEDs), with device structures shown in Fig. 2a and b, respectively. Each device was simultaneously fabricated on glass/ITO, CPI/AgNW, and scattering pCPI/CPI/AgNW substrate for direct comparison. First, a modified PEDOT:PSS (Heraeus) layer was deposited on each substrate via spin coating (2 krpm for 60 s) and annealed on a hot plate for 10 min at 150 °C. This is to achieve not only an efficient hole injection from ITO or AgNW, but a more uniform distribution of current in which sparse AgNWs are filled in with conductive PEDOT:PSS. The

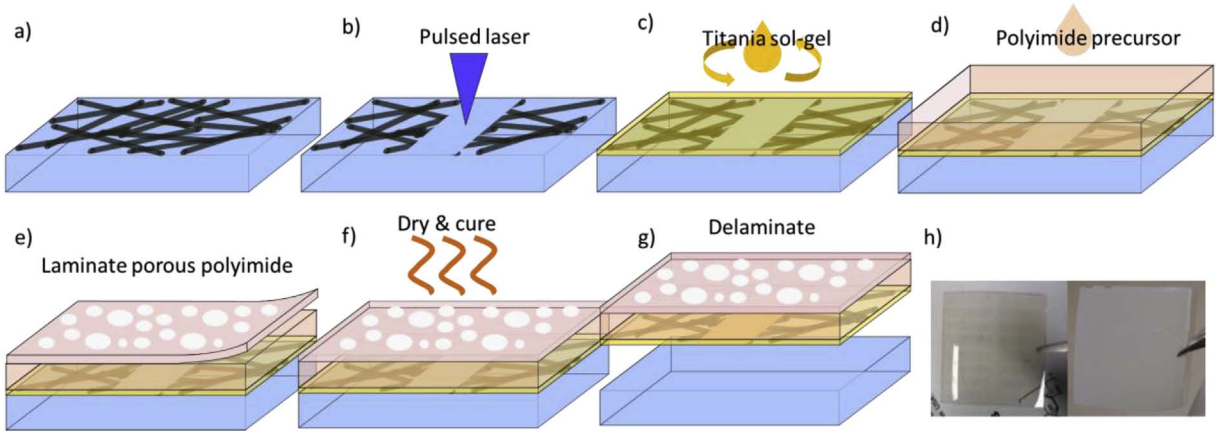

Fig. 1. a) AgNWs are spin coated on a clean glass slide. b) A UV pulsed laser is used to ablate the AgNWs for device integration. c) Titania sol-gel is spin coated. d) Colorless polyimide precursor is blade coated and dried under vacuum. e) Freestanding porous colorless polyimide is prepared and laminated on the polyimide precursor film. Note that this step is omitted for CPI/TiO_2/AgNW control substrates. f) The glass/AgNW/TiO_2/CPI/pCPI stack is imidized. g) The flexible substrate is delaminated from the glass carrier. h) Photographs of 3 × 3 cm^2 substrates of CPI/TiO_2/AgNW (left) and the hazy pCPI/CPI/TiO_2/AgNW (right).

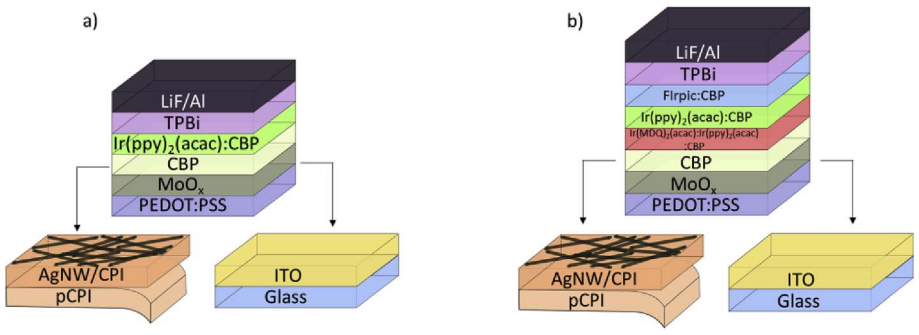

Fig. 2. Schematic device structures of a) green, and b) white phosphorescent OLEDs used in this work.

PEDOT:PSS is modified with 0.01% (v/v) Triton X-100 (Sigma Aldrich) to improve wetting on CPI/AgNW substrates. The modified PEDOT:PSS forms a uniform 60 nm layer when directly spin coated on the CPI/AgNW substrates without surface pretreatment such as O_2 plasma. The glass/ITO control substrates (Lumtec, 135 nm thick ITO) were sonicated in acetone and isopropanol and were treated with 5 min O_2 plasma before spin coating. The substrates were then transferred to a vacuum thermal evaporation chamber (EvoVac, Angstrom, base pressure of $\sim 1 \times 10^{-7}$ Torr) for organic film growth. For the green OLEDs, we evaporated 5 nm MoO_3 (Alfa Aesar), 20 nm CBP (4,4′-bis(N-carbazolyl)-1,1′-biphenyl), 15 nm CBP doped with 8% $Ir(ppy)_2(acac)$ (bis[2-(2-pyridinyl-N)phenyl-C]), 80 nm TPBi (2,2′,2”-(1,3,5-benzinetriyl)-tris(1- phenyl-1H-benzimidazole), and 1.2 nm LiF. For the white OLEDs, we evaporated 5 nm MoO_3, 20 nm CBP, 15 nm CBP doped with 5% $Ir(ppy)_2(acac)$ and 5% $Ir(MDQ)_2(acac)$ (bis(2-methyldibenzo[f,h]quinoxaline)(acetylacetonate)iridium(III)), 3 nm CBP doped with 8% $Ir(ppy)_2(acac)$, 8 nm CBP doped with 20% FIrpic (bis[2-(4,6-difluorophenyl)pyridinato-C2,N](picolinato)iridium(III)), 80 nm TPBi, and 1.2 nm LiF. 100 nm aluminum (R.D. Mathis) contacts were evaporated for both the green and the white OLEDs. All materials were purchased from Nichem unless mentioned otherwise. The fabricated OLEDs were tested in a nitrogen glovebox with a Keithley 2400 source-measure unit, a calibrated silicon photodiode (Thorlabs), and a fiber optic spectrophotometer (StellarNet Inc.). The mechanical bending test was also carried out in the nitrogen glovebox, using a motorized translation stage (MTS50-X8, Thorlabs).

3. Results and discussion

3.1. Characterization of scattering polyimide substrates

We characterize our AgNW TCEs as they are employed within a device. It is found that the electrodes have a low sheet resistance of approximately 25 Ω/□, indicating that the thin TiO_2 layer is indeed effective at protecting the AgNWs during the imidization at 360 °C. This is also confirmed by the scanning electron microscope (SEM) image of the CPI/AgNW substrate (Fig. 3a), which shows that the AgNWs are visibly intact and not broken up into droplets. Another important aspect of AgNW TCE desirable in this work is low haze, which allows us to eliminate any outcoupling enhancement from light scattering by the AgNWs. Metallic AgNWs are typically efficient scatterers compared to planar ITO films with low haze (< 1%) [37], but haze can be minimized by employing small-diameter AgNWs (30 nm in this work) as haze increases exponentially with nanowire diameter [38]. Moreover, simulations and experiments have shown that a high aspect ratio (length/diameter) is required to simultaneously optimize sheet resistance and optical transmittance of metal nanowires [39], and thus we use the AgNWs with a large aspect ratio of approximately 5000. The optical characterization data in Fig. 3b shows that the CPI/AgNW substrates exhibit an extremely low haze (2% average) and > 85% transmission averaged over the wavelength range from 450 to 800 nm. On the other hand, the pCPI/CPI/AgNW scattering substrate exhibits high broadband haze (> 75%) across the visible spectrum. The large haze is attributed to the scattering from the pCPI film, as the haze of the AgNWs is relatively small. The efficient scattering is enabled by the air voids that present a large index contrast when embedded in the relatively high-index CPI ($n > 1.66$ at 400 nm, Fig. S2). The morphology of the voids is shown in the SEM image of the pCPI surface (Fig. 3c) in which micron-sized depressions as well as nanoscale voids are present. It should be noted that these voids are not only of various shapes and sizes but also distributed randomly within the pCPI. This presents a significant advantage over nanostructures created by lithography which are typically periodic and ordered features that are not suited for applications requiring broadband enhancement. Furthermore, focused ion beam (FIB) etching of the pCPI/CPI (Fig. 3d) shows its porous cross section and its interface with the underlying neat CPI, as indicated by the dashed line. In order to create an optically and chemically bonded interface between the neat CPI and pCPI, we imidize the two layers simultaneously. To do so, the pCPI film is laminated on the backside of CPI/AgNW after the stack has been dried under vacuum at a slightly elevated temperature (80 °C). Due to the residual solvent, the laminated pCPI film is partially re-dissolved before the pCPI/CPI/AgNW stack is imidized. This is indicated by the decrease in thickness for the standalone pCPI film (8 μm) compared to the pCPI film laminated on CPI (6.3 μm). Therefore, we assume that the pCPI/CPI interface is intimate and crosslinked together due to partial re-dissolution at the interface. This assumption appears to be valid as the cross-section of the pCPI/CPI interface in Fig. 3d appears smooth and defect-free.

3.2. Outcoupling enhancement in green and white PHOLEDs on scattering substrates

The ability of the pCPI scattering layer to increase outcoupling is tested by fabricating green and white PHOLEDs. The green PHOLEDs fabricated on CPI/AgNW substrates with and without pCPI show nearly identical electrical behavior while the pCPI-assisted device shows improved luminance, resulting in 36.4% EQE compared to 25.5% without pCPI, and 21% on glass/ITO (at 1 mA cm^{-2}). This is an improvement of 1.73× compared to the glass/ITO device and 1.42× compared to the CPI/AgNW device. The power efficiency at 100 cd m^{-2} increases from 63 lm/W (glass/ITO) to 74 lm/W (CPI/AgNW) to 104 lm/W (pCPI/CPI/AgNW), an enhancement of 1.65× compared to the glass/ITO device and 1.4× compared to the CPI/AgNW device. See Fig. S3a for the performance of the other devices on the same pCPI/CPI/AgNW substrate. In addition, the angular emission profile (Fig. 4d) of the pCPI/CPI/AgNW device is closer to Lambertian compared to those of the glass/ITO and the CPI/AgNW devices. This suggests that the pCPI scatters and outcouples the rather directional emission generated in the weak microcavity device in a more random fashion, resulting in a more Lambertian output. The improved efficiency observed in the CPI/AgNW device compared to the glass/ITO device is likely owing to less efficient hole injection from the lower work function AgNW compared to ITO and reduced waveguiding loss via elimination of the high-index ITO. The latter point combined with the higher index contrast at the CPI/air

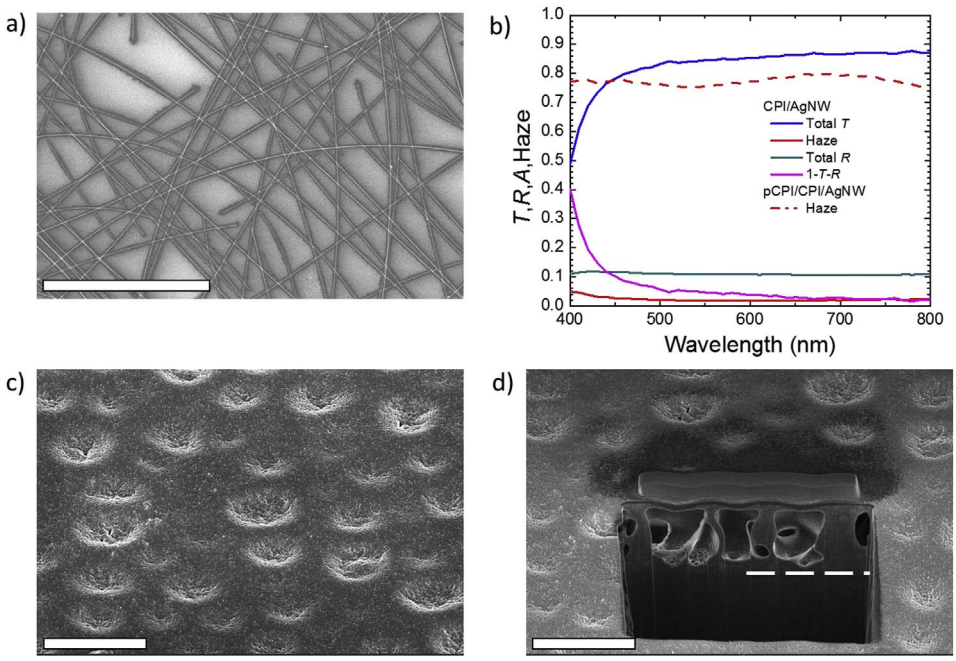

Fig. 3. a) SEM image of AgNWs embedded in CPI. b) Transmission (T), reflection (R), absorption ($A = 1 - T - R$), and haze of a control CPI/AgNW film, and haze of a pCPI/CPI/AgNW film. c) SEM image of pCPI. d) SEM image of pCPI at 52° with its cross-section exposed by focused ion beam etching. A thin layer of platinum was deposited to protect the pCPI surface, and the dashed line shows the interface between CPI and pCPI. All scale bars are 10 μm.

interface leads to a higher portion of the light trapped in the CPI/AgNW substrate. We believe that the increased substrate loss presents an environment in which residual scattering from the sparse AgNWs as well as any inherent surface roughness or bending can more easily cause unintentional improvement in outcoupling efficiency of the CPI/AgNW devices.

We show analogous efficiency enhancements for the white PHOLEDs, indicating broadband outcoupling enhancement ability of the pCPI scattering layer. The EQE of the pCPI-assisted device is 24.3% (at 1 mA cm^{-2}), which is 1.51× larger compared to the CPI/AgNW device (16%) and a 1.68× enhancement compared to the glass/ITO device (14.4%). The PE of the pCPI-assisted device (32.4 lm/W, at 100 cd m^{-2}) is an enhancement of 1.74× compared to the glass/ITO device (18.4 lm/W) and 1.59× larger than the CPI/AgNW device (20.4 lm/W). See Fig. S3b for the performance of white OLEDs on pCPI/CPI/AgNW substrates fabricated from multiple batches. The angular emission profiles (Fig. 5d) show that the pCPI/CPI/AgNW device slightly differs from the CPI/AgNW device, likely due to scattering from the pCPI film redirecting the propagation of the internally emitted light out of the substrate. The effect of randomly scattered emission due to the pCPI film is most evident in the electroluminescence (EL) spectra measured at various viewing angles (Fig. S4); both the glass/ITO device and the CPI/AgNW device exhibit significant shifts in spectra as the viewing angle is changed from 0° to 70°, but the pCPI/CPI/AgNW device shows virtually identical spectra independent of viewing angle. The effect of scattering from the pCPI film and its impact on the

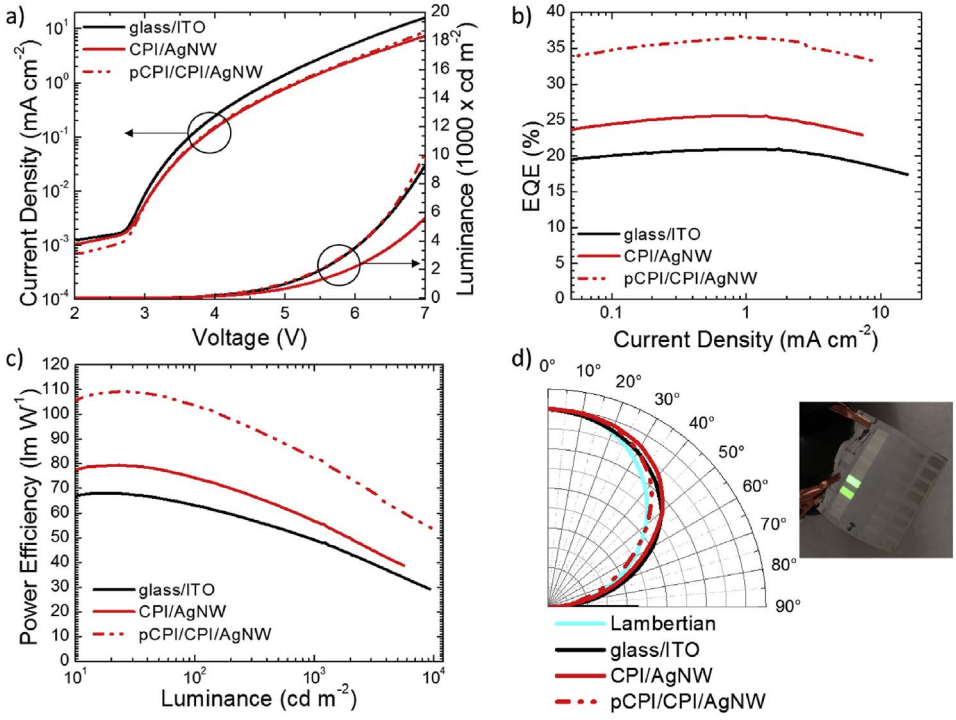

Fig. 4. Device characteristics for green PHOLEDs on various substrates: a) Current density (J) and forward luminance (L) vs. voltage; b) EQE vs. J; c) Power efficiency (PE) vs. L; d) Angular emission profiles and photograph of two lit devices on a 3 × 3 cm^2 pCPI/CPI/AgNW substrate.

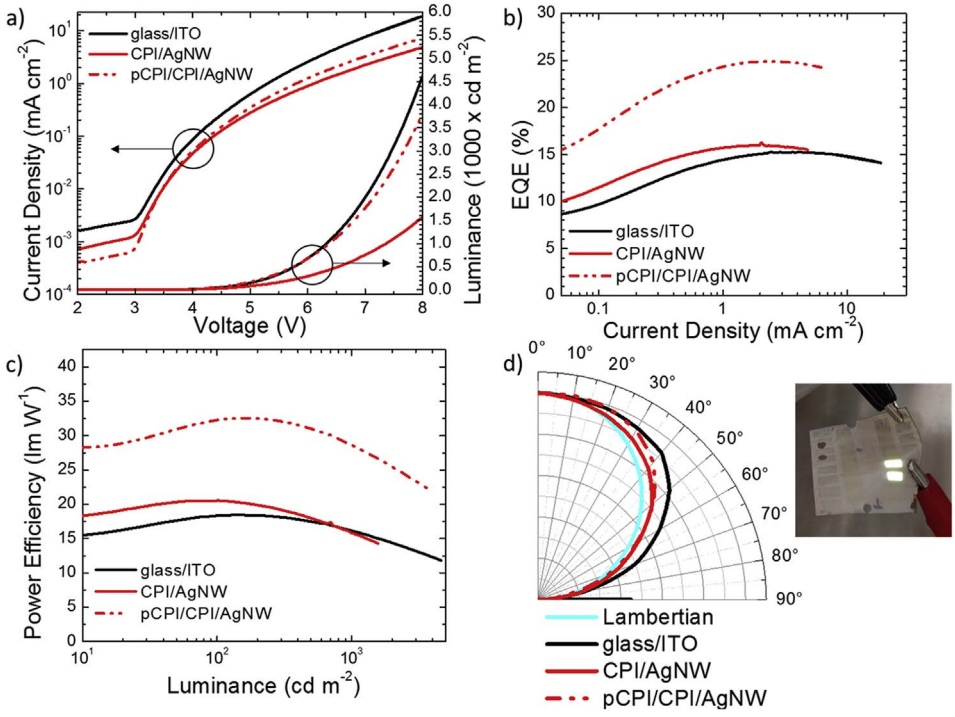

Fig. 5. a) Current density (J) and forward luminance (L) vs. voltage for white PHOLEDs on various substrates. b) EQE vs. J. c) PE vs. L. d) Angular emission profiles and photograph of two lit white OLEDs on a 3 × 3 cm^2 pCPI/CPI/AgNW substrate.

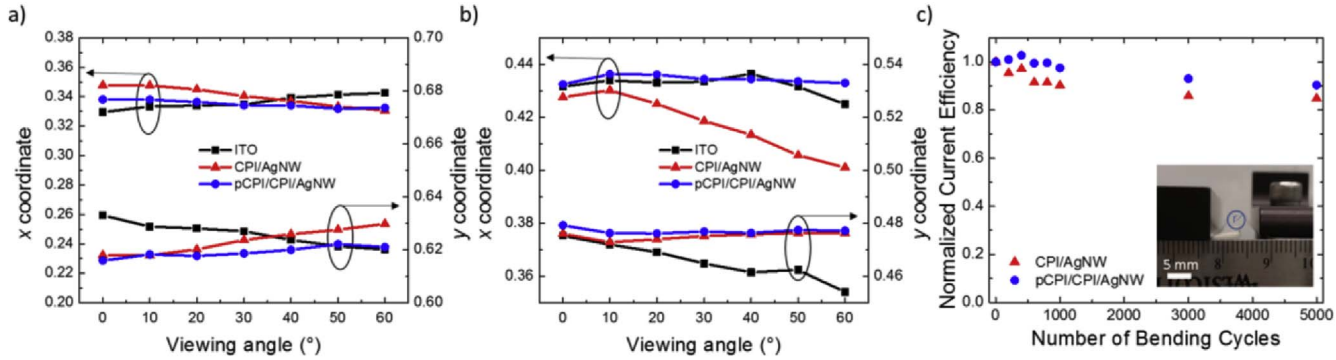

Fig. 6. CIE1931 x and y coordinates of the a) green PHOLEDs, and b) white PHOLEDs fabricated on various substrates, vs. viewing angle. c) normalized peak current efficiency as a function of bending cycles (bending radius, r = 2 mm) and photograph of a CPI/AgNW device bent at a 2 mm radius.

improved color uniformity over viewing angles is quantified by CIE1931 x and y coordinates for the green OLEDs and the white OLEDs (Fig. 6a and b, respectively), computed from their corresponding EL spectra (Figs. S4 and S5, respectively). Clearly, the pCPI-assisted device has the smallest changes across 0°–60°. The change of the x and y coordinates from 0° to 60°, $|\Delta(x,y)|$, is (0.006,0.005) for the green OLED on the pCPI-assisted device and (0.001,0.004) for the white OLED on the pCPI-assisted device which is a significant improvement from the glass/ITO devices with $|\Delta(x,y)|$ of (0.013,0.013) and (0.048,0.018) for the green and white OLEDs, respectively. The shifts in the forward EL spectra of the white OLEDs fabricated on various substrates also result in different correlated color temperature and CRI, as the CRI is 80 (3583 K) for the glass/ITO device, 78 (3652 K) for the CPI/AgNW device, and 77 (3592 K) for the pCPI/CPI/AgNW device. The change in CRI across various substrates can be understood as a direct result of the CPI/AgNW substrates having a different microcavity environment than the glass/ITO substrate due to the difference in refractive indices as well as optical properties of the AgNW vs. ITO TCEs. Further modification of the far-field propagation occurs in the optically thick substrates and their interface with air. In the case of the pCPI-assisted substrate, the random scattering of the internally generated light results in white OLED with excellent color uniformity, which is an important aspect in general for lighting. Higher CRI values can be realized by fine-tuning the spectral content of the OLEDs or by using another set of emitters, as the pCPI/CPI substrate has high transmission and broadband haze over the full visible spectrum.

The change in outcoupling efficiency of the pCPI scattering layer with mechanical stress is tested by repeatedly bending the white OLEDs on a CPI/AgNW substrate and a pCPI/CPI/AgNW substrate. The bending test was carried out by simultaneously bending the white OLEDs on the CPI/AgNW substrate and the pCPI/CPI/AgNW substrate at a ~2 mm radius (r), with the substrates (CPI or pCPI/CPI) on the outside of the bending radius, hence exposing the pCPI film to tensile stress. The peak current efficiency (CE) of the OLEDs was measured as a function of bending cycles and was normalized by the initial current efficiency of each device. As shown in Fig. 6c, the CE decreases slowly with the number of bending cycles up to 5000 at which point the normalized value falls to approximately 85% and 90% for the CPI/AgNW device and the pCPI/CPI/AgNW device, respectively. This means that although the white OLEDs do degrade due to mechanical stress, the degree of degradation differs only slightly with and without the pCPI scattering layer. In fact, the normalized CE is consistently higher for the pCPI-assisted white OLED. In other words, the outcoupling efficiency of the pCPI film in the forward direction remains unharmed after 5000

bending cycles at $r \sim 2$ mm. Furthermore, no significant morphological change was observed in the pCPI film after the bending test.

4. Conclusion

In summary, we introduce composite silver nanowire electrodes embedded in flexible porous colorless polyimide substrates that efficiently outcouple substrate loss in both monochromatic and white OLEDs. The composite scattering substrates improve the EQE of a green OLED and a white OLED by 74% and 68%, respectively. The outcoupling enhancement originates from a thin film of porous colorless polyimide on the substrate backside which exhibits broadband haze (> 75%) due to a large index contrast between the colorless polyimide and air voids. The color uniformity between viewing angles 0° and 60° is also significantly improved, as shown by a reduced $|\Delta(x,y)|$ shift of (0.006,0.005) for the green OLED and (0.001,0.004) for the white OLED. Moreover, the pCPI scattering layer is mechanically robust in which its outcoupling efficiency remains unharmed after 5000 bending cycles at a 2 mm bending radius. Hence, the composite AgNW/scattering polyimide substrates fabricated without costly lithography provide a thermally, chemically, and mechanically robust flexible platform for efficient white OLEDs for future lighting applications.

Acknowledgement

We acknowledge funding for this work from the DOE EERE SSL Program [Award #DE-EE0006672]. B.P.R. acknowledges support from a 3M Nontenured Faculty Award and DARPA Young Faculty Award. R.F. and C.B.A. acknowledge the support of the National Science Foundation via the MRSEC at Princeton [DMR-0819860] and the usage of the PRISM Imaging and Analysis Center.

Appendix A. Supplementary data

Supplementary data related to this article can be found at http://dx.doi.org/10.1016/j.orgel.2017.09.042.

References

[1] C. Adachi, M.A. Baldo, M.E. Thompson, S.R. Forrest, Nearly 100% internal phosphorescence efficiency in an organic light emitting device, J. Appl. Phys. 90 (2001) 5048–5051.
[2] M.A. Baldo, D.F. O'Brien, Y. You, A. Shoustikov, S. Sibley, M.E. Thompson, S.R. Forrest, Highly efficient phosphorescent emission from organic electroluminescent devices, Nature 395 (1998) 151–154.
[3] H. Kaji, H. Suzuki, T. Fukushima, K. Shizu, K. Suzuki, S. Kubo, T. Komino, H. Oiwa, F. Suzuki, A. Wakamiya, Y. Murata, C. Adachi, Purely organic electroluminescent material realizing 100% conversion from electricity to light, Nat. Commun. 6 (2015) 8476.
[4] T.-A. Lin, T. Chatterjee, W.-L. Tsai, W.-K. Lee, M.-J. Wu, M. Jiao, K.-C. Pan, C.-L. Yi, C.-L. Chung, K.-T. Wong, C.-C. Wu, Sky-blue organic light emitting diode with 37% external quantum efficiency using thermally activated delayed fluorescence from spiroacridine-triazine hybrid, Adv. Mater. 28 (2016) 6976–6983.
[5] M. Morales-Masis, F. Dauzou, Q. Jeangros, A. Dabirian, H. Lifka, R. Gierth, M. Ruske, D. Moet, A. Hessler-Wyser, C. Ballif, An indium-free anode for large-area flexible OLEDs: defect-free transparent conductive zinc tin oxide, Adv. Funct. Mater. 26 (2016) 384–392.
[6] H. Kang, I. Kang, J. Han, J.B. Kim, D.Y. Lee, S.M. Cho, J.H. Cho, Flexible and mechanically robust organic light-emitting diodes based on photopatternable silver nanowire electrodes, J. Phys. Chem. C 120 (2016) 22012–22018.
[7] J.A. Spechler, T.-W. Koh, J.T. Herb, B.P. Rand, C.B. Arnold, A transparent, smooth, thermally robust, conductive polyimide for flexible electronics, Adv. Funct. Mater. 25 (2015) 7428–7434.
[8] H.G. Im, S.H. Jung, J. Jin, D. Lee, J. Lee, D. Lee, J.Y. Lee, I.D. Kim, B.S. Bae, Flexible transparent conducting hybrid film using a surface-embedded copper nanowire network: a highly oxidation-resistant copper nanowire electrode for flexible optoelectronics, ACS Nano 8 (2014) 10973–10979.
[9] J.H.M. Maurer, L. González-García, B. Reiser, I. Kanelidis, T. Kraus, Templated self-assembly of ultrathin gold nanowires by nanoimprinting for transparent flexible electronics, Nano Lett. 16 (2016) 2921–2925.
[10] N. Li, S. Oida, G.S. Tulevski, S.-J. Han, J.B. Hannon, D.K. Sadana, T.-C. Chen, Efficient and bright organic light-emitting diodes on single-layer graphene electrodes, Nat. Commun. 4 (2013) 1–7.
[11] T.-H. Han, Y. Lee, M.-R. Choi, S.-H. Woo, S.-H. Bae, B.H. Hong, J.-H. Ahn, T.-W. Lee, Extremely efficient flexible organic light-emitting diodes with modified graphene anode, Nat. Photonics 6 (2012) 105–110.
[12] J. Gao, X. Mu, X.-Y. Li, W.-Y. Wang, Y. Meng, X.-B. Xu, L.-T. Chen, L.-J. Cui, X. Wu, H.-Z. Geng, Modification of carbon nanotube transparent conducting films for electrodes in organic light-emitting diodes, Nanotechnology 24 (2013) 435201.
[13] J. Li, L. Hu, L. Wang, Y. Zhou, G. Grüner, T.J. Marks, Organic light-emitting diodes having carbon nanotube anodes, Nano Lett. 6 (2006) 2472–2477.
[14] R. Meerheim, M. Furno, S. Hofmann, B. Lüssem, K. Leo, Quantification of energy loss mechanisms in organic light-emitting diodes, Appl. Phys. Lett. 97 (2010) 25–28.
[15] H. Benisty, R. Stanley, M. Mayer, Method of source terms for dipole emission modification in modes of arbitrary planar structures, J. Opt. Soc. Am. A 15 (1998) 1192–1201.
[16] M.C. Gather, S. Reineke, Recent advances in light outcoupling from white organic light-emitting diodes, J. Phot. Energy 5 (2015) 57607.
[17] F. So, J. Kido, P. Burrows, Organic light-emitting devices for solid-state lighting, MRS Bull. 33 (2008) 663–669.
[18] J.W. Park, D.C. Shin, S.H. Park, Large-area OLED lightings and their applications, Semicond. Sci. Technol. 26 (2011) 34002.
[19] H.Y. Xiang, Y.Q. Li, L. Zhou, H.J. Xie, C. Li, Q.D. Ou, Chen, L. Sen, C.S. Lee, S.T. Lee, J.X. Tang, Outcoupling-enhanced flexible organic light-emitting diodes on ameliorated plastic substrate with built-in indium-tin-oxide-free transparent electrode, ACS Nano 9 (2015) 7553–7562.
[20] L. Zhou, H.-Y. Xiang, S. Shen, Y.-Q. Li, J.-D. Chen, H.-J. Xie, I.A. Goldthorpe, L.-S. Chen, S.-T. Lee, J.-X. Tang, High-performance flexible organic light-emitting diodes using embedded silver network transparent electrodes, ACS Nano 8 (2014) 12796–12805.
[21] Y. Luo, C. Wang, L. Wang, Y. Ding, L. Li, B. Wei, J. Zhang, Flexible organic light-emitting diodes with enhanced light out-coupling efficiency fabricated on a double-sided nanotextured substrate, ACS Appl. Mater. Interfaces 6 (2014) 10213–10219.
[22] Y.Y. Kim, J.J. Park, S.J. Ye, W.J. Hyun, H.-G. Im, B.-S. Bae, O.O. Park, Novel microlens arrays with embedded Al $_2$ O $_3$ nanoparticles for enhancing efficiency and stability of flexible polymer light-emitting diodes, RSC Adv. 6 (2016) 65450–65458.
[23] L. Li, J. Liang, S.-Y. Chou, X. Zhu, X. Niu, ZhibinYu, Q. Pei, A solution processed flexible nanocomposite electrode with efficient light extraction for organic light emitting diodes, Sci. Rep. 4 (2015) 4307.
[24] S. Gim, I. Lee, J.Y. Park, J. Lee, Spontaneously embedded scattering structures in a flexible substrate for light extraction, Small 13 (2017) 1604168.
[25] T.W. Koh, J.A. Spechler, K.M. Lee, C.B. Arnold, B.P. Rand, Enhanced outcoupling in organic light-emitting diodes via a high-index contrast scattering layer, ACS Photonics 2 (2015) 1366–1372.
[26] G.R. Guillen, Y. Pan, M. Li, E.M.V. Hoek, Preparation and characterization of membranes formed by nonsolvent induced phase separation: a review, Ind. Eng. Chem. Res. 50 (2011) 3798–3817.
[27] H. Go, T.-W. Koh, H. Jung, C.Y. Park, T.-W. Ha, E.M. Kim, M.H. Kang, Y.H. Kim, C. Yun, Enhanced light-outcoupling in organic light-emitting diodes through a coated scattering layer based on porous polymer films, Org. Electron. 47 (2017) 117–125.
[28] T. Matsumoto, D. Mikami, T. Hashimoto, M. Kaise, R. Takahashi, S. Kawabata, Alicyclic polyimides – a colorless and thermally stable polymer for opto-electronic devices, J. Phys. Conf. Ser. 187 (2009) 12005.
[29] Y. Guo, H. Song, L. Zhai, J. Liu, S. Yang, Synthesis and characterization of novel semi-alicyclic polyimides from methyl-substituted tetralin dianhydride and aromatic diamines, Polym. J. 44 (2012) 718–723.
[30] C.-P. Yang, R.-S. Chen, K.-H. Chen, Light-colored and soluble fluorinated polyimides based on 2-trifluoromethyl-4,4′-diaminodiphenyl ether and various aromatic dianhydrides, Colloid Polym. Sci. 281 (2003) 505–515.
[31] S. Ando, T. Matsuura, S. Sasaki, Coloration of aromatic polyimides and electronic properties of their source materials, Polym. J. 29 (1997) 69–76.
[32] K.-H. Ok, J. Kim, S.-R. Park, Y. Kim, C.-J. Lee, S.-J. Hong, M.-G. Kwak, N. Kim, C.J. Han, J.-W. Kim, Ultra-thin and smooth transparent electrode for flexible and leakage-free organic light-emitting diodes, Sci. Rep. 5 (2015) 9464.
[33] K.-B. Kim, Y.-H. Tak, Y.-S. Han, K.-H. Baik, M.-H. Yoon, M.-H. Lee, Relationship between surface roughness of indium tin oxide and leakage current of organic light-emitting diode, Jpn. J. Appl. Phys. 42 (2003) L438–L440.
[34] W.-F. Xu, M.-C. Tsai, P.-H. Fu, T.-Y. Huang, S.-J. Yang, W.-C. Tian, C.-W. Chu, D.-W. Huang, P.-K. Wei, Efficiency enhancement of organic solar cells using peroxo-polytitanic acid coated silver nanowires as transparent electrodes, RSC Adv. 5 (2015) 18990–18996.
[35] D.P. Langley, M. Lagrange, G. Giusti, C. Jiménez, Y. Bréchet, N.D. Nguyen, D. Bellet, Metallic nanowire networks: effects of thermal annealing on electrical resistance, Nanoscale 6 (2014) 13535–13543.
[36] E.C. Garnett, W. Cai, J.J. Cha, F. Mahmood, S.T. Connor, M. Greyson Christoforo, Y. Cui, M.D. McGehee, M.L. Brongersma, Self-limited plasmonic welding of silver nanowire junctions, Nat. Mater. 11 (2012) 241–249.
[37] X. Yu, X. Yu, J. Zhang, D. Zhang, J. Ni, H. Cai, D. Zhang, Y. Zhao, Investigation of light transmission and scattering properties in silver nanowire mesh transparent electrodes, Mater. Lett. 145 (2015) 219–233.
[38] S. Ye, A.R. Rathmell, Z. Chen, I.E. Stewart, B.J. Wiley, Metal nanowire networks: the next generation of transparent conductors, Adv. Mater. 26 (2014) 6670–6687.
[39] R.M. Mutiso, M.C. Sherrott, A.R. Rathmell, B.J. Wiley, K.I. Winey, Integrating simulations and experiments to predict sheet resistance and optical transmittance in nanowire films for transparent conductors, ACS Nano 7 (2013) 7654–7663.